Evaluation of Biological Dose for ARIES-CS and Comparison with Approximate Contact Dose Approach

A. Robinson, L. El-Guebaly, D. Henderson

May 2010

UWFDM-1375

FUSION TECHNOLOGY INSTITUTE

UNIVERSITY OF WISCONSIN

MADISON WISCONSIN

Evaluation of Biological Dose for ARIES-CS and Comparison with Approximate Contact Dose Approach

A. Robinson, L. El-Guebaly, D. Henderson

Fusion Technology Institute
University of Wisconsin
1500 Engineering Drive
Madison, WI 53706

http://fti.neep.wisc.edu

May 2010

UWFDM-1375

Abstract

Every few years, maintenance will be required to replace the plasma facing components of any fusion power plant. To come up with a realistic maintenance scheme, an accurate method of evaluating the biological dose is needed. In some studies, the simple and quick approach of the contact dose for a specific component was used to estimate the biological dose. This method doesn't take radiation from nearby components into account and the accuracy of its methodology is questionable. The more accurate multi-step method, which involves transporting the delayed gammas from induced activation in the forward or adjoint mode, is able to take radiation from all surrounding components into account. In this report, the biological dose was evaluated with the adjoint method at selected radial locations of ARIES-CS, and then compared to the contact dose of the nearest component to determine the accuracy of the contact dose method. Our results indicate that the contact dose could be off by an order of magnitude.

1. Introduction

For the biological dose comparison, we selected the latest design in the ARIES series [1]: ARIES-CS – a compact stellarator design [2] developed in 2006 by the ARIES team to enhance the attractiveness of stellarators as a commercial power plant. The first wall (FW) of ARIES-CS and all surrounding in-vessel components conform to the plasma, as shown in Fig. 1, and deviate from the uniform toroidal shape in order to achieve compactness. The power core can be divided into two distinct sets of components: replaceable components and permanent components. The replaceable components, which consist of the FW, blanket, and back wall, are located between the plasma and the shield. This region is scheduled for replacement every 3.9 full power years (FPY). The permanent components consist of the shield, manifolds, vacuum vessel (VV), magnet, cryostat, and bioshield. These components are designed to last 40 FPY, the life of the plant. Figure 2 shows a simplified radial build for the ARIES-CS design with these two sets of components highlighted [3]. This radial build is typical for any fusion power plant, except for the toroidal field magnets of ARIES-CS that are continuous and not discrete as in tokamaks. The main structural material of ARIES-CS is F82H – a low-activation ferritic steel (FS). The dimensions and compositions of all components are documented in Reference 3. As Fig. 2

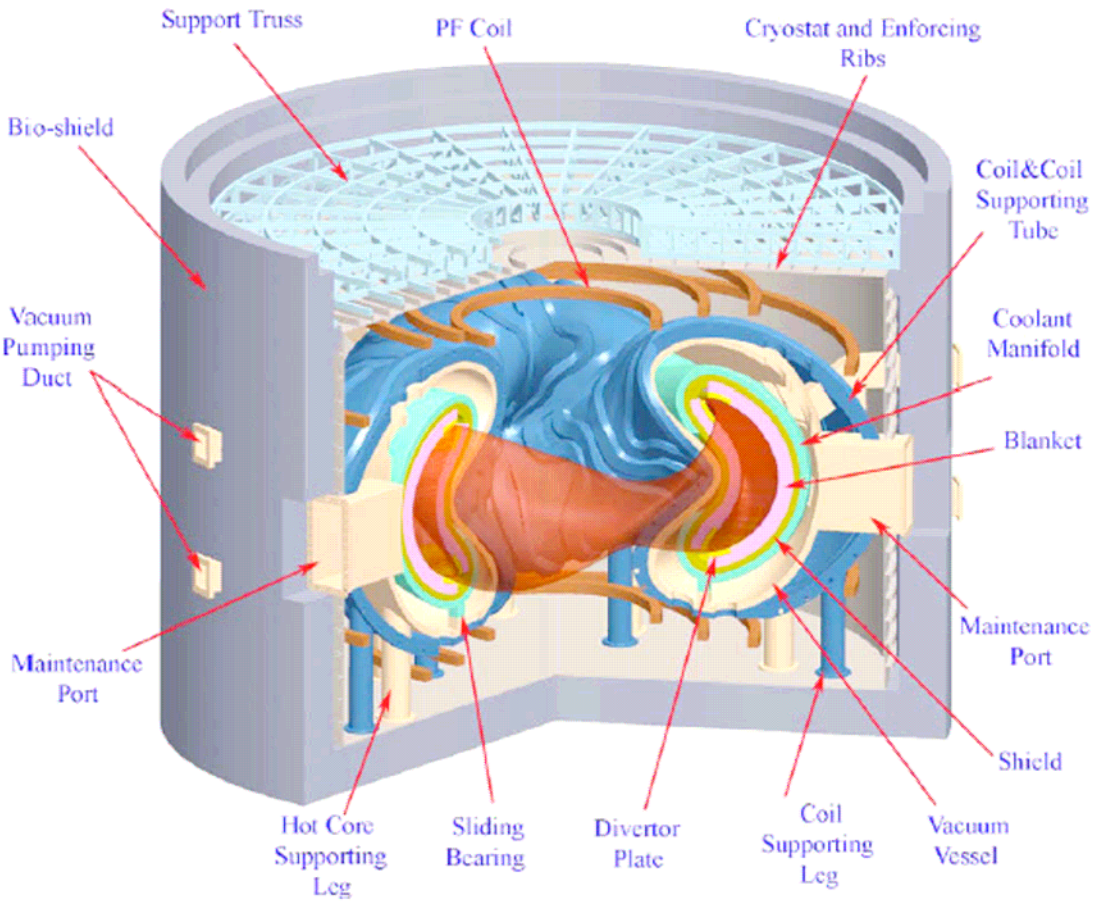

Figure 1. Isometric view of ARIES-CS [2].

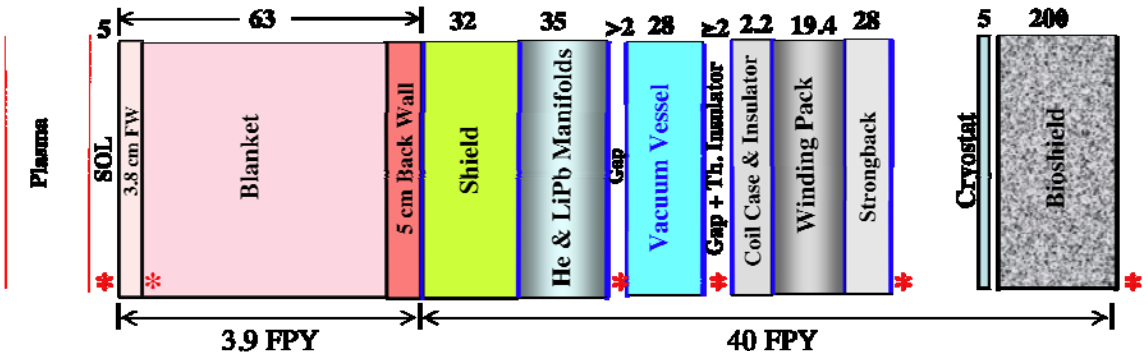

Figure 2. ARIES-CS radial build [3]. Locations where the biological doses were calculated are indicated with red asterisks. Thicknesses are in centimeters.

indicates, the ARIES-CS cylindrical model was assumed to have no penetrations or assembly gaps to simplify biological dose calculations. Therefore, the effect of streaming neutrons was not considered. In general, all penetrations tend to increase the calculated biodose, unless well shielded.

2. Methodology, Codes, and Data

The methodology used for the activation and dose rate calculations is a multi-step (forward or adjoint) method that has been developed and extensively used by the UW–Madison Fusion Technology Institute (FTI) neutronics group, dating back to the mid-1970s [4-33]. The forward and adjoint methodology has been incorporated into several activation codes that were developed by FTI over a period of 30 years of fusion research work [4,10,11,12,13,20,26,27]. Since its early use by FTI, the forward and/or adjoint method has been used by other fusion research centers at national laboratories and educational institutions [34-58]. This multi-step method has been coined the rigorous method. The dose rate is found by using either the forward gamma transport method or the adjoint method in combination with the gamma ray flux-to-dose rate conversion factors [59,60]. The forward method involves the creation of the decay gamma energy and spatial distributions (gamma source) by an activation code and the further transport of these gammas from their point of generation to other regions and zones of the geometric model via a rigorous transport calculation. The adjoint method involves running the transport code in adjoint mode to generate the adjoint gamma flux with a dose detector in the region or point of interest, then running the activation code to generate the gamma source in each interval. Historically, the biological dose (biodose) calculations have been performed with a variety of radioactivity (activation) codes with coupling schemes for the neutron and decay gamma transports and auxiliary codes for dose computation in one and multi-dimensional configurations: 1-D [4,6-9,16-19,21-25,28-33], 2-D [10-15,34,35,38,39], and 3-D [20,26,27,36,37,40-58].

The multi-step method is in contrast to another commonly used approximate method known as the contact dose method, which is based on the FISPACT [61] methodology and ANS

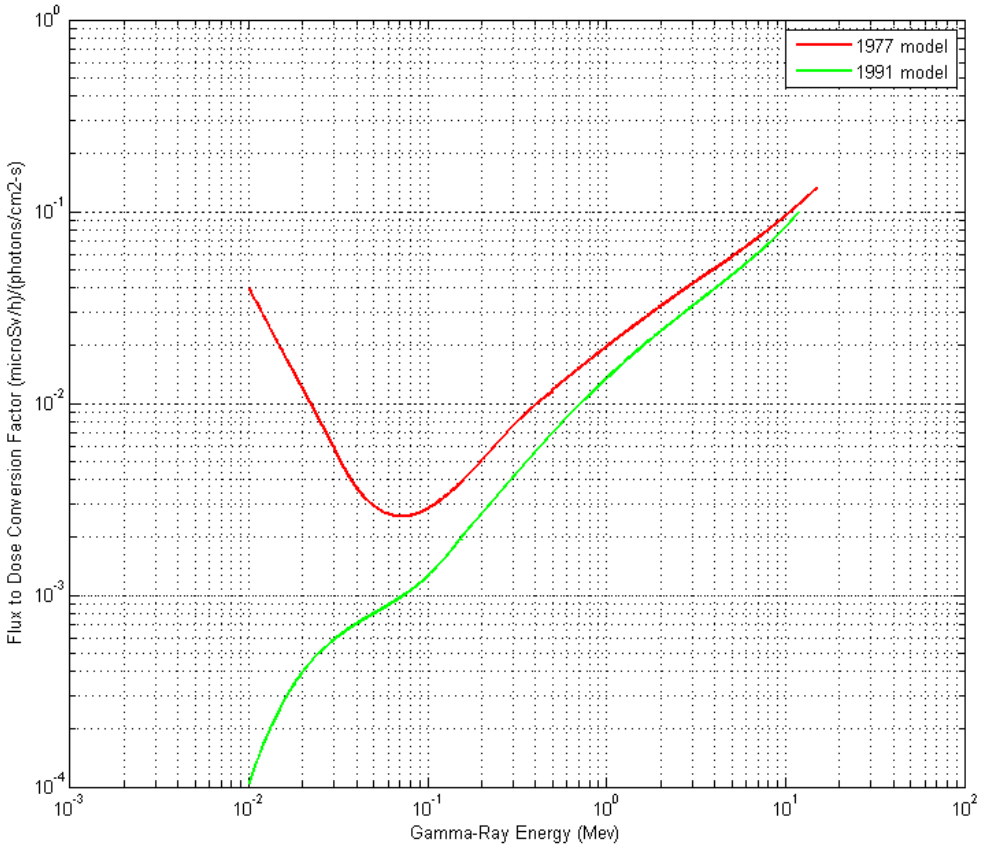

Figure 3. 1977 and 1991 ANSI/ANS gamma flux-to-dose conversion factor models. The 1977 model is for gamma energies of .01 MeV to 15 MeV [59] and the 1991 model is for gamma energies of .01 MeV to 12 MeV [60].

conversion factors [62]. The FISPACT methodology is a simple, quick method that evaluates the decay gamma dose at the surface of a semi-infinite slab using material-specific attenuation coefficients. Its roots are from the early days of dose calculation when specific geometry kernels/expressions and buildup factors were used to compute the biological dose [63]. This method evaluates the contact dose for a specific component and is unable to take gamma radiation from surrounding activated components into account. This constraint has raised questions regarding its accuracy in estimating the biological dose during maintenance near points of interest in any fusion device. To assess the accuracy of the approximate contact dose method, it was compared to the more accurate multi-step method where the surrounding components contribute to the biodose during maintenance.

Because the multi-step method requires gamma flux-to-dose conversion factors, the two published conversion factor models were examined. The first model is from the 1977 ANSI/ANS report [59] and the second model is from the 1991 ANSI/ANS report [60]. These two models are shown in Fig. 3. Note that the 1991 model should result in a lower dose and, unlike the 1977 model, there is no significant contribution to the dose from gammas with low energies below 0.1 MeV. Even though the 1991 model represents a newer version of the conversion factors, it was officially withdrawn by ANSI as an American National Standard in 2001. ANSI believes the

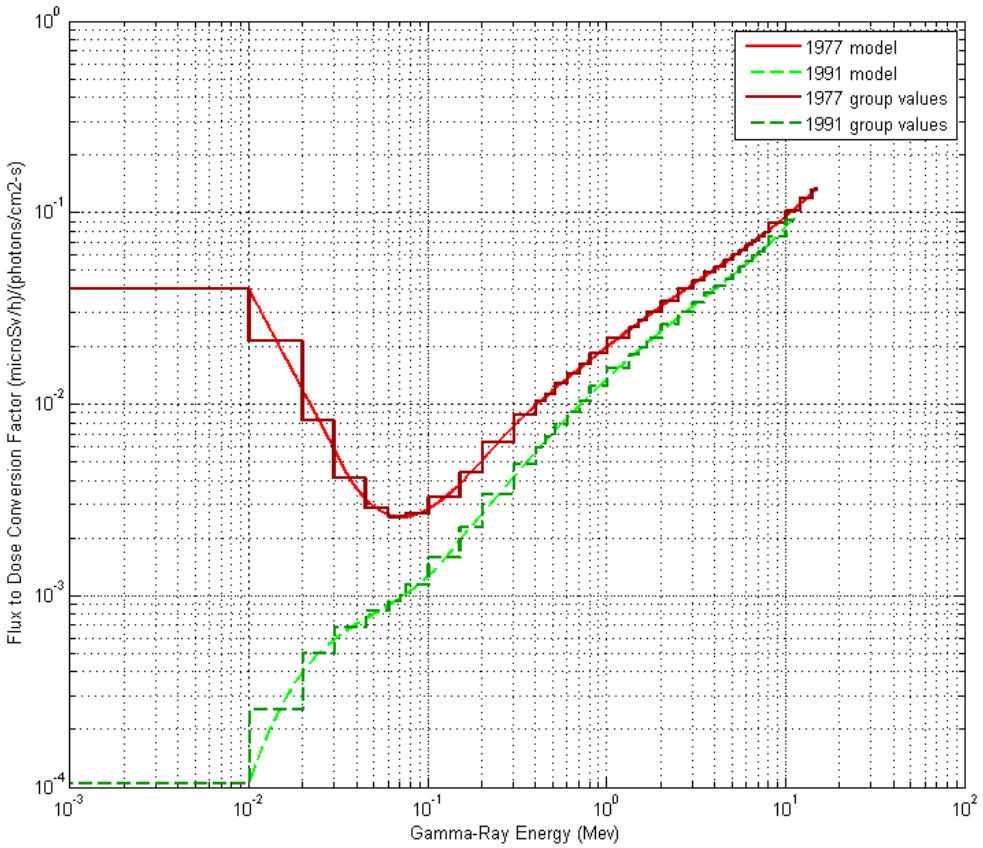

Figure 4. 1977 and 1991 ANSI/ANS flux-to-dose conversion factor models and the generated 42 group flux-to-dose conversion factors.

information contained in the 1991 standard is correct, but a formal ANS review to determine its accuracy has yet to be performed. Before starting the biodose analysis, both models were examined to determine which one would be best for our study.

The transport code used for the neutron and gamma transport calculations, both in the forward and adjoint modes, was the DANTSYS discrete ordinates, neutral particle code [64]. The code was run in the $S_{12}P_5$ approximation using the 1-D cylindrical equivalent geometry model of Fig. 2. The cross section data library used was the coupled neutron and gamma photon FENDL-2.1 library with 175 neutron and 42 gamma groups [65]. The neutron source was placed in the middle of the plasma and the source neutrons have an energy of 14.1 MeV. The source intensity was 1.3 x 10^{17} n/cm·s that corresponds to an average neutron wall loading of 2.6 MW/m^2 at the FW. The activation and final adjoint dose rate calculations were performed with the ALARA activation code [26,27]. Data inputs to this code are the IAEA activation cross-section library and the FENDL-2 decay data library [66]. The elemental compositions of the blanket materials can be found in Reference 3. The operation schedule reflects the 85% availability of ARIES-CS and the ALARA code accurately models all operation and down times for the replaceable and permanent components.

Table 1. 42 gamma group flux-to-dose conversion factors. The top 2 groups (> 16 MeV) are not included because of lack of data and they are not useful for fusion decay gammas.

Upper Bound (MeV)	1977 µSv/h per $g/cm^2 \cdot s$	1991 µSv/h per $g/cm^2 \cdot s$	Upper Bound (MeV)	1977 µSv/h per $g/cm^2 \cdot s$	1991 µSv/h per $g/cm^2 \cdot s$
16	1.325E-01	-	1	1.833E-02	1.229E-02
14	1.178E-01	-	0.8	1.604E-02	1.040E-02
12	1.026E-01	9.093E-02	0.7	1.442E-02	9.077E-03
10	8.772E-02	7.522E-02	0.6	1.281E-02	7.791E-03
8	7.847E-02	6.596E-02	0.512	1.202E-02	7.161E-03
7.5	7.478E-02	6.238E-02	0.51	1.128E-02	6.721E-03
7	7.110E-02	5.883E-02	0.45	1.032E-02	5.931E-03
6.5	6.743E-02	5.532E-02	0.4	8.759E-03	4.837E-03
6	6.375E-02	5.184E-02	0.3	6.306E-03	3.369E-03
5.5	6.007E-02	4.835E-02	0.2	4.391E-03	2.287E-03
5	5.601E-02	4.485E-02	0.15	3.277E-03	1.570E-03
4.5	5.227E-02	4.132E-02	0.1	2.682E-03	1.131E-03
4	4.832E-02	3.771E-02	0.075	2.578E-03	9.925E-04
3.5	4.412E-02	3.399E-02	0.07	2.601E-03	9.290E-04
3	3.960E-02	3.009E-02	0.06	2.844E-03	8.242E-04
2.5	3.469E-02	2.594E-02	0.045	4.115E-03	6.798E-04
2	3.019E-02	2.218E-02	0.03	8.267E-03	5.003E-04
1.66	2.731E-02	1.978E-02	0.02	2.144E-02	2.556E-04
1.5	2.536E-02	1.815E-02	0.01	3.961E-02	2.597E-05
1.34	2.430E-02	1.726E-02	0.001	-	-
1.33	2.205E-02	1.539E-02			

From both of these models, 42 gamma group flux-to-dose conversion factors were generated based on the FENDL gamma group structure. In Fig. 4, the group values are superimposed on top of the respective flux-to-dose conversion factor curves of Fig. 3. All gamma groups that exceeded the energy limits of their respective model were set to the value of nearest energy group that fell within the model limits. This is most important for the lowest gamma group (0.001 MeV to .01 MeV) because of the potential for gamma radiation to fall within this low

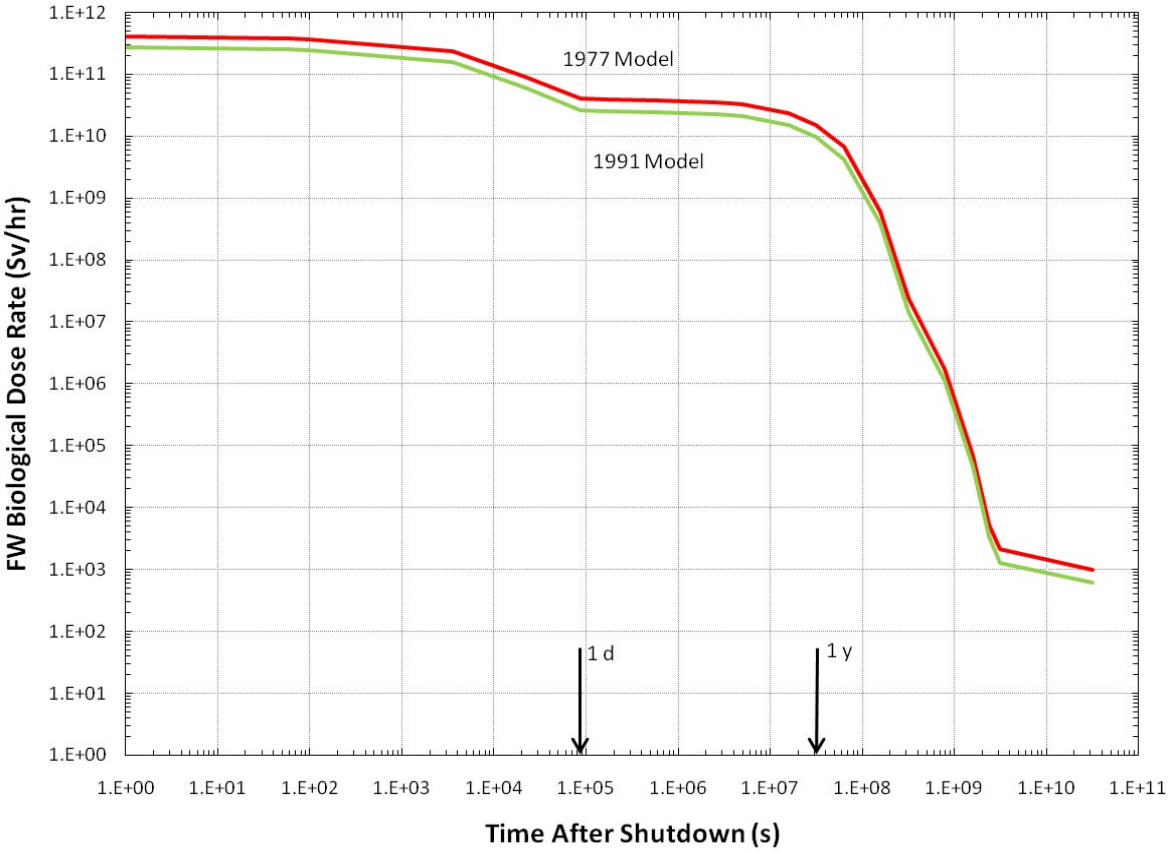

Figure 5. The biological dose rate just outside the FW using the 1977 and 1991 42 group gamma flux-to-dose conversion factors.

energy range. This approximation does not affect the highest energy groups beyond 15 MeV for the 1977 model and beyond 12 MeV for the 1991 model. Ultimately, the flux-to-dose conversion factors were set to zero for higher energy groups above these energies because fusion decay gammas do not normally reach these high energies. The group flux-to-dose conversion factors shown in Fig. 4 are also listed in Table 1 for convenience.

As Fig. 4 indicates, the 1977 ANSI/ANS gamma flux-to-dose conversion factor model provides a more conservative result than the 1991 model. Therefore, a test case was run to determine the difference between the two models in biodoses calculated at the FW. The detailed step-by-step procedure used to acquire the data for this test case (and all subsequent cases) is provided in the Appendix. Figure 5 shows the biological dose calculated behind the FW using both models. Based on the results of this test case, the biological dose calculated with the 1977 model was roughly between 50% and 60% higher than the 1991 model at all times after shutdown. Therefore, in order to be conservative, the 1977 gamma flux-to-dose conversion factors were used in all subsequent calculations.

Before any comparisons were done, the effectiveness of the LiPb breeder as an effective gamma shield during maintenance was explored. Figure 6 shows an expanded view of the blanket that was used in the ARIES-CS radial build. In Figure 6, there are two regions containing LiPb: blanket and manifolds. Normally, these regions would be drained out before maintenance.

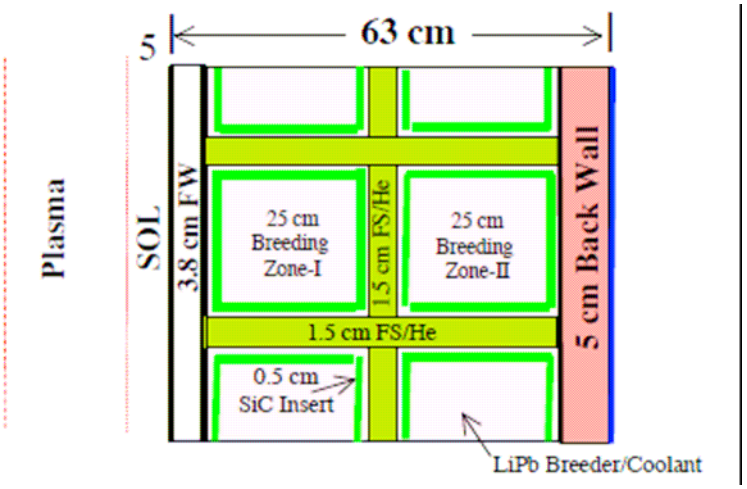

Figure 6. Expanded view of ARIES-CS replaceable components.

Therefore, the LiPb in these regions was initially left out of the adjoint gamma transport calculations. Comparing the biological dose calculations where the LiPb was left in to the original calculations, no major differences were found. It seems that the Pb effectively absorbs almost all gammas generated in the LiPb. Therefore, all of the following results were acquired for the most practical case without any LiPb present during maintenance, i.e., no LiPb in the replaceable components during the adjoint gamma transport calculation.

3. Results

Using the adjoint method for determining the biological dose, several comparisons were made to the contact dose at different radial locations within ARIES-CS. Figure 2 shows the locations where the biological dose was calculated and compared to the contact dose of the nearest component.

The first comparison was made at the front (plasma side) of the FW and right behind the FW. Figure 7 shows the results of the comparison. The contact dose method underestimates the biological dose at both sides of the FW. Originally, it was thought that gamma contributions from the surrounding components would be significant, which would explain the contact dose difference observed in Fig. 7. However, Table 2 shows that this is not the case as the FW itself generates more than 90% of the biodose. At one day after shutdown (the time of interest for maintenance), only 4% and 9% of the biological dose calculated before and behind the FW, respectively, come from the blanket. Most of the blanket contributions come from gamma decay by Mn-54. About 96% of the Mn-54 produced in the blanket is a result of neutron reactions with Fe-54 in the F82H FS and 4% of the Mn-54 produced is a result of neutron reactions with the Fe-56 in FS. In the FW, 90% of the Mn-54 produced is a result of neutron reactions with Fe-54 and 7% of the Mn-54 produced is a result of neutron reactions with Fe-56. Clearly, the contribution from components surrounding the FW is not large enough to explain the differences shown in Fig. 7. Therefore, it is the contact dose methodology itself that is causing the difference in the FW biodose results.

Table 2. Isotopic contributions to biological dose rate calculated behind the FW at one day after shutdown. Mn-54 in both the FW and the blanket is the largest contributor to the biological dose. Mn-54 in the blanket has been highlighted to emphasize that it is the highest contributor from components surrounding the FW.

	Dose Rate (Sv/h)			
isotope	FW	SiC	Breeding Zone	Total
Cr-51	9.29E+02 (2.30%)	1.97E-05 (0.00%)	2.57E+01 (0.06%)	9.54E+02 (2.36%)
Mn-52	3.60E+02 (0.89%)	8.37E-06 (0.00%)	2.46E+01 (0.06%)	3.84E+02 (0.95%)
Mn-54	2.97E+04 (73.51%)	9.34E-04 (0.00%)	3.17E+03 (7.84%)	3.29E+04 (81.35%)
Mn-56	3.60E+02 (0.89%)	1.08E-05 (0.00%)	4.56E+01 (0.11%)	4.06E+02 (1.00%)
Fe-59	3.39E+02 (0.84%)	8.51E-05 (0.00%)	6.26E+01 (0.15%)	4.02E+02 (0.99%)
Co-58	2.76E+02 (0.68%)	3.41E-03 (0.00%)	3.06E+01 (0.08%)	3.06E+02 (0.76%)
Y-88	2.73E+03 (6.74%)	8.91E-05 (0.00%)	4.51E-04 (0.00%)	2.73E+03 (6.74%)
Ta-182	1.04E+03 (2.57%)	2.00E-04 (0.00%)	1.11E+02 (0.27%)	1.15E+03 (2.84%)
W-187	4.83E+02 (1.19%)	6.98E-05 (0.00%)	4.56E+01 (0.11%)	5.28E+02 (1.31%)
traces	5.74E+02 (1.42%)	4.41E+01 (0.11%)	6.91E+01 (0.17%)	6.88E+02 (1.70%)
Total	3.68E+04 (91.03%)	4.41E+01 (0.11%)	3.59E+03 (8.86%)	4.05E+04 (100.00%)

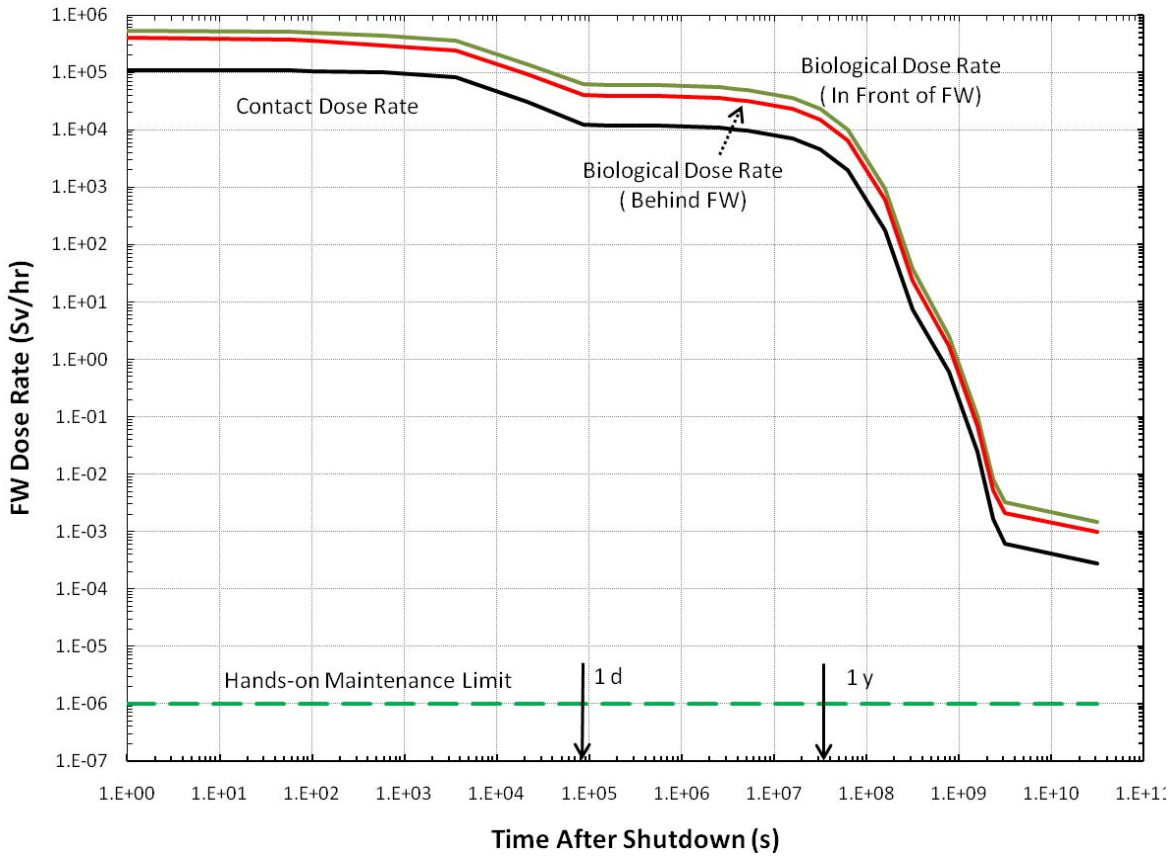

Figure 7. Comparison of the contact dose rate of the FW to the biological dose rate on the plasma side of the FW and just behind the FW.

The next comparison was made just in front and behind the VV. Figure 8 shows the results of the comparison. As expected, the contact dose rate lies between the two biological dose curves. For equipment accessing the front of the VV, the contact dose method underestimates the biodose rate by an order of magnitude at one day after shutdown. For equipment accessing the back of the VV, the contact dose method overestimates the biodose by more than an order of magnitude at one day after shutdown. The contact dose rate of the inner coil case was also compared to the biological dose rate behind the VV. Again, the contact dose method underestimated the biological dose rate at the front of the magnet by ~ two orders of magnitude at one day after shutdown. Gammas from nearby components were looked at to explain the differences observed. Table 3 summarizes the contributions to the biological dose behind the VV at one day after shutdown. The VV itself accounts for ~ 93% of the calculated biological dose behind the VV, with roughly 5% of the biological dose coming from the manifolds, 1.5% from the inner coil case, and < 0.5% from the winding pack (WP). Within the manifolds, Ta-182 is responsible for most of the biological dose. All of the Ta-182 production in the Manifolds is a result of neutron reactions with the 0.02 wt% Ta (Ta-181) in the F82H FS. Within the VV, Ta-182 and W-187 are responsible for most of the biological dose. Their production is solely the result of (n,gamma) reactions with the 0.02 wt% Ta and 2 wt% W, respectively, in the F82H FS. These small contributions (~7%) from components surrounding the VV are not enough to account for the large differences between the contact doses and the biological dose calculated

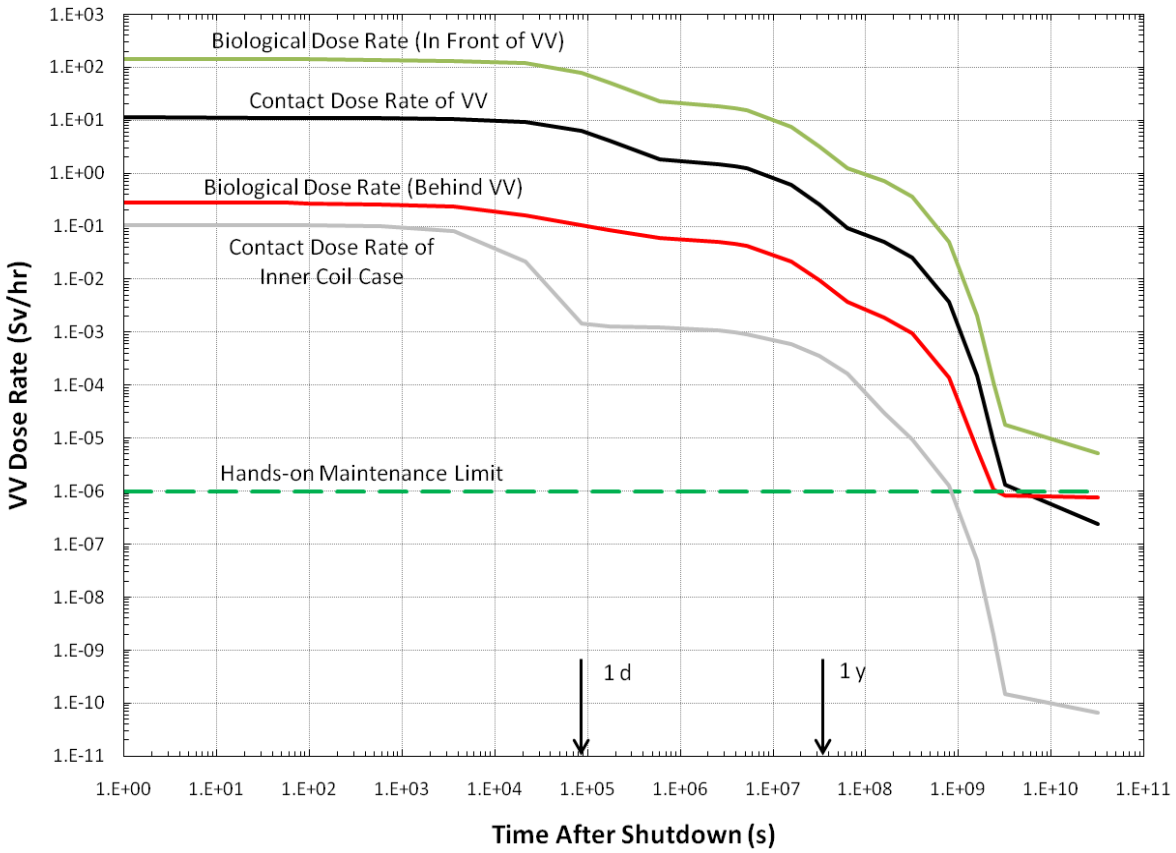

Figure 8. Comparison of the contact dose rate of the VV to the biological dose rate just in front of the VV and just outside of the VV. The contact dose rate of the inner coil case has also been added for comparison.

behind the VV. Therefore, it is the contact dose methodology itself that is causing the difference at the VV.

The next comparison was made just behind the magnet and Fig. 9 shows the results. Note that, at 1-10 days, all doses exceed the hands-on maintenance limit of 1 μSv/h. This design limit is 10 fold lower than the absolute hands-on limit (10 μSv/h), to take into consideration the "As Low As Reasonably Achievable" principle. As the figure indicates, the contact dose rate of the cryostat underestimates the biological dose rate until 1 day. The contact dose rate of the 28 cm thick strongback (made of JK2LB steel) agrees well with the biological dose rate at 1-10 days after shutdown. After 10 days, the contact dose rate of the strongback underestimates the biological dose rate. The contributions of the surrounding components may help explain these unexpected results. At one day, the main contributors to the biological dose rate are given in Table 4. It is clear that the cryostat is actually the main contributor to the biological dose behind the magnet, accounting for 74% of the calculated biological dose. Only 20% of the dose comes from the strongback and the remaining from the bioshield. In this regard, the good agreement between the contact dose of the strongback and the biological dose is surprising. Excluding the cryostat and bioshield contributions, the contact dose of the strongback actually overestimates the biodose behind the magnet.

Table 3. Isotopic contributions to biological dose rate calculated behind the VV at one day after shutdown. Ta-182 in the manifolds has been highlighted because it is the largest contributor to the biological dose from components surrounding the VV.

	Dose Rate (Sv/h)					
isotope	Manifolds	VV	Inner Coil Case	GFF Poly	WP	Total
Mn-54	4.09E-06 (0.00%)	9.77E-04 (0.92%)	8.40E-04 (0.79%)	- (0.00%)	4.04E-05 (0.04%)	1.86E-03 (1.75%)
Fe-59	9.98E-04 (0.94%)	5.41E-03 (5.07%)	3.61E-05 (0.03%)	- (0.00%)	1.89E-06 (0.00%)	6.45E-03 (6.05%)
Co-60	3.96E-04 (0.37%)	3.09E-03 (2.90%)	3.13E-05 (0.03%)	- (0.00%)	3.77E-05 (0.04%)	3.56E-03 (3.33%)
Ta-182	3.29E-03 (3.09%)	4.48E-02 (42.03%)	- (0.00%)	- (0.00%)	- (0.00%)	4.81E-02 (45.12%)
W-187	5.86E-04 (0.55%)	4.48E-02 (41.98%)	- (0.00%)	- (0.00%)	- (0.00%)	4.54E-02 (42.53%)
Traces	2.15E-06 (0.00%)	1.19E-04 (0.11%)	7.83E-04 (0.73%)	1.80E-06 (0.00%)	4.05E-04 (0.38%)	1.31E-03 (1.23%)
Total	5.28E-03 (4.95%)	9.92E-02 (93.01%)	1.69E-03 (1.59%)	1.80E-06 (0.00%)	4.85E-04 (0.45%)	1.07E-01 (100.00%)

Interestingly, the contact dose rate of the cryostat (made of 304-SS) very closely matches both the biological dose rate (between one day and 100 years) and the contact dose of the strongback (between 1 and 30 days). From 2 days to 100 years, the 304-SS cryostat is the main contributor to the biological dose rate behind the strongback (see Fig. 10). The contact dose of the cryostat is as high as that of the strongback after one day because the 304-SS of the cryostat is more radioactive than the low-activation JK2LB steel developed specifically for fusion magnets. Inside the 304-SS cryostat, Co-60 is the main contributor to the biological dose, which is produced by neutron absorption by the 0.1 wt% Co in the 304-SS. Inside the bioshield, Na-24 is the main contributor to the biological dose, which is produced by neutron absorption by the 1.7 wt% Na in the concrete.

To examine the impact of the cryostat materials on the biological dose rate behind the strongback, we replaced the 304-SS by the JK2LB steel of the magnet and by the MF82H of the blanket/shield/VV. Figure 11 displays the results for all three steels. Evidently, the biological dose rate could be reduced by more than 3 fold after one day if the cryostat is made of JK2LB

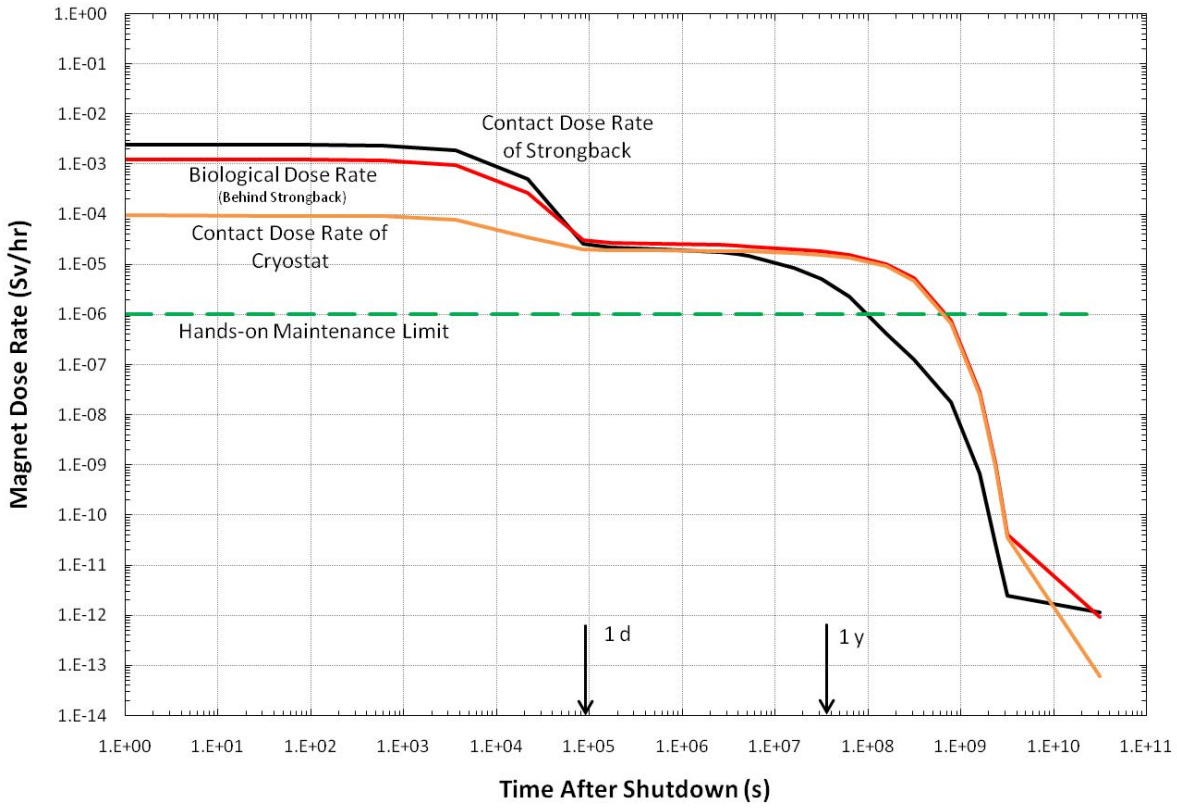

Figure 9. Comparison of the contact dose rate of the strongback to the biological dose rate just outside the strongback. The contact dose rate of the cryostat has also been added to further aid in the comparison.

steel instead of 304-SS. At one day, the contribution of the MF82H cryostat to the biological dose rate is high (~ 71%) while that of the JK2LB cryostat is relative low (~35%).

The last comparison was made just outside of the bioshield (see Fig. 12). The contact dose of the last 50 cm of the bioshield overestimates the biological dose by up to an order of magnitude. Incidentally, these results confirm the safe exposure of workers and the public outside the bioshield to the higher radiation level (~10^5 fold) during operation, provided that all penetrations and access ports are well shielded against streaming radiation.

The contributions to the biological dose were analyzed in detail at one day after shutdown because that time is relevant to maintenance. However, all times after shutdown should be looked at to better understand the differences between the multi-step method and the contact dose method. Figure 13 shows the contributions of the FW, VV, and strongback to the biological dose rates calculated behind the FW, behind the VV, and behind the magnet, respectively. This figure reaffirms that, in most cases, the component nearest to where the biological dose rate is calculated has the largest contribution to the biological dose rate. Therefore, the order of magnitude or more differences between the contact dose rate and the biological dose rate are mainly due to the contact dose methodology itself. However, there is at least one case (behind the magnet) where gammas from nearby components appear to cause a notable difference. From

Table 4. Isotopic contributions to biological dose rate calculated behind the strongback of the magnet at one day after shutdown. Co-60 in the cryostat and Na-24 in the bioshield have been highlighted to emphasize that they are the largest contributors to the biological dose rate behind the strongback of the magnet.

	Dose Rate (Sv/h)			
isotope	Strongback	Cryostat	Bioshield	Total
Na-24	- (0.00%)	- (0.00%)	1.73E-06 (5.70%)	1.73E-06 (5.70%)
Cr-51	1.97E-07 (0.65%)	3.38E-07 (1.11%)	- (0.00%)	5.36E-07 (1.76%)
Mn-54	1.22E-06 (4.01%)	1.94E-07 (0.64%)	1.89E-09 (0.01%)	1.41E-06 (4.65%)
Mn-56	1.74E-06 (5.74%)	1.22E-07 (0.40%)	3.72E-09 (0.01%)	1.87E-06 (6.15%)
Fe-59	5.00E-07 (1.65%)	7.77E-07 (2.56%)	6.38E-08 (0.21%)	1.34E-06 (4.42%)
Co-58	1.89E-06 (6.22%)	1.16E-06 (3.83%)	- (0.00%)	3.05E-06 (10.05%)
Co-60	5.12E-08 (0.17%)	1.96E-05 (64.56%)	- (0.00%)	1.96E-05 (64.73%)
Mo-99	3.99E-07 (1.32%)	1.13E-07 (0.37%)	- (0.00%)	5.13E-07 (1.69%)
traces	9.28E-08 (0.31%)	1.49E-07 (0.49%)	1.34E-08 (0.04%)	2.55E-07 (0.84%)
Total	6.09E-06 (20.06%)	2.24E-05 (73.97%)	1.81E-06 (5.98%)	3.03E-05 (100.00%)

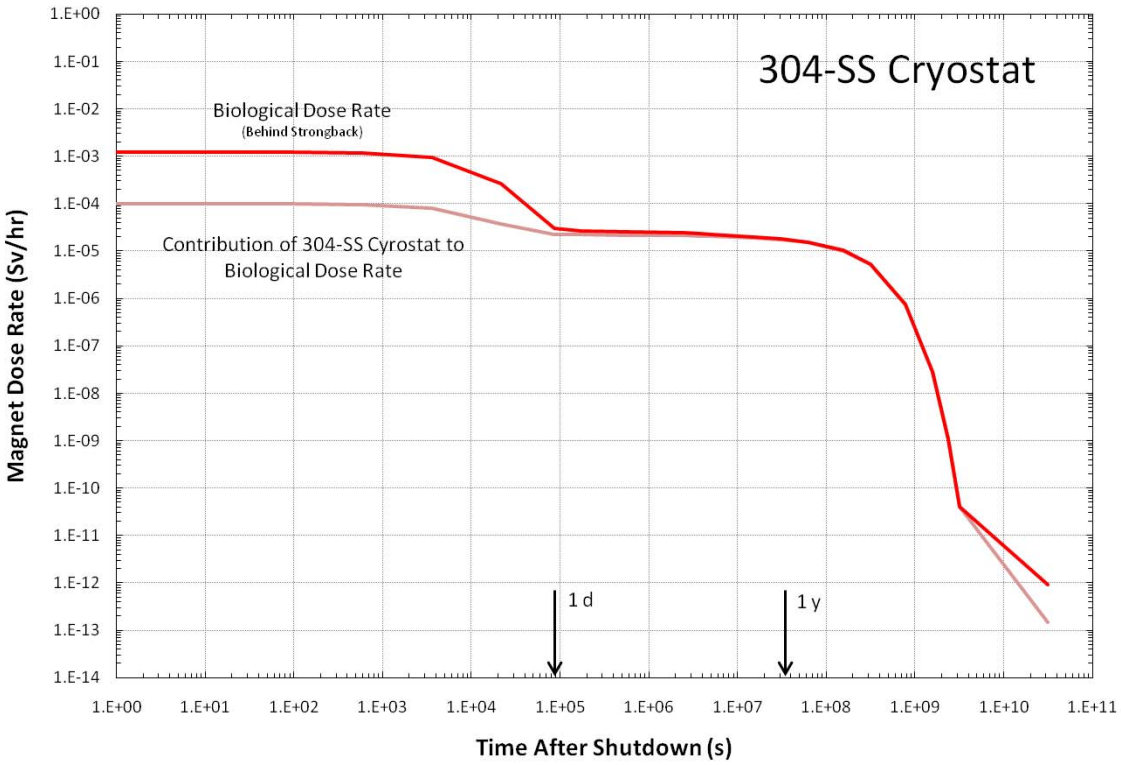

Figure 10. Contribution of 304-SS cryostat to biological dose rate behind strongback of magnet.

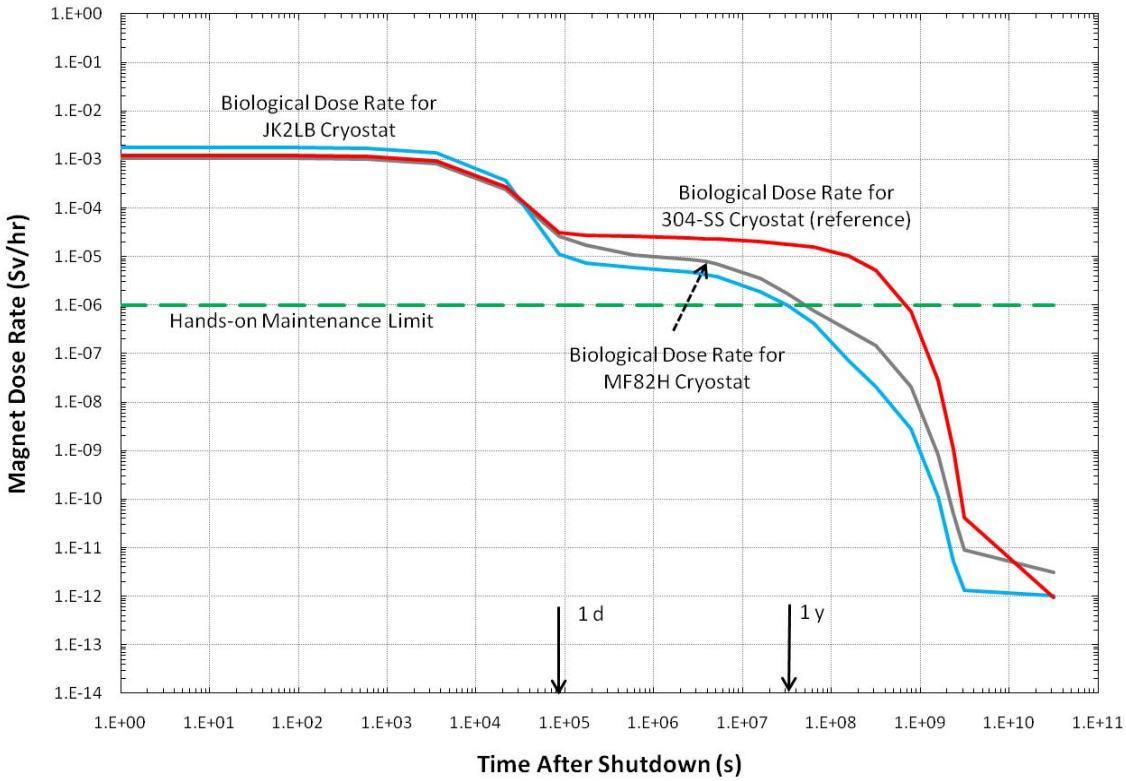

Figure 11. Sensitivity of biological dose rate behind strongback to cryostat materials.

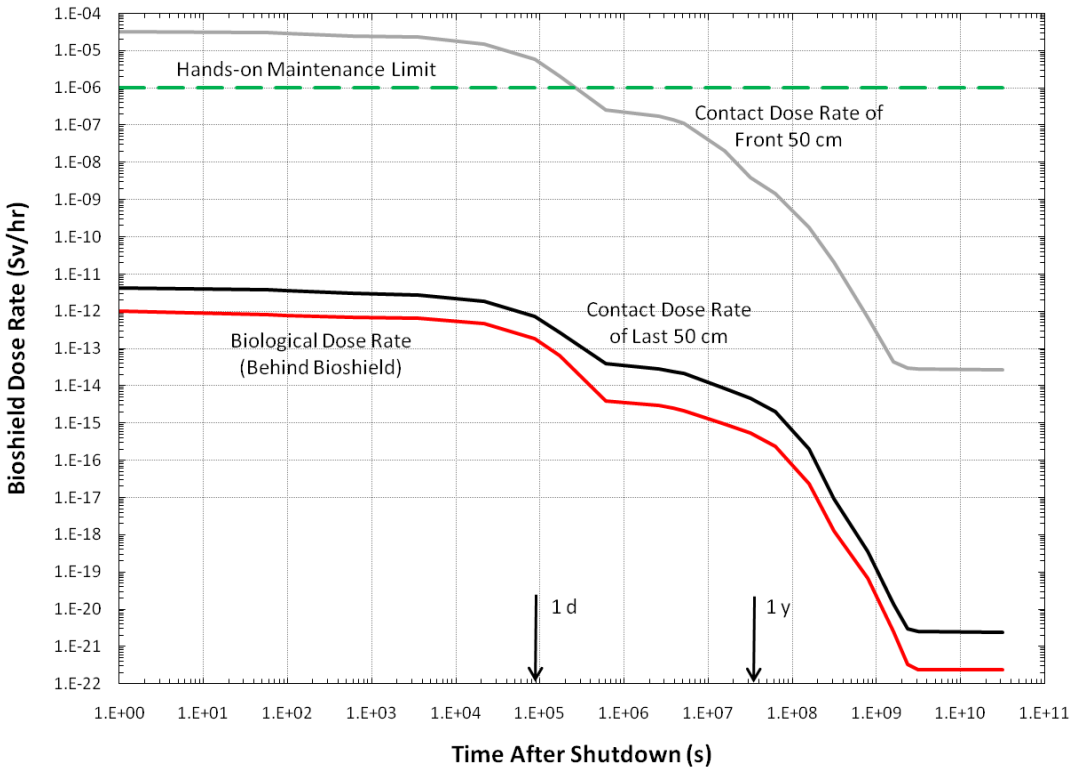

Figure 12. Comparison of the contact dose rates of the front and last 50 cm of the bioshield to the biological dose rate just outside the bioshield.

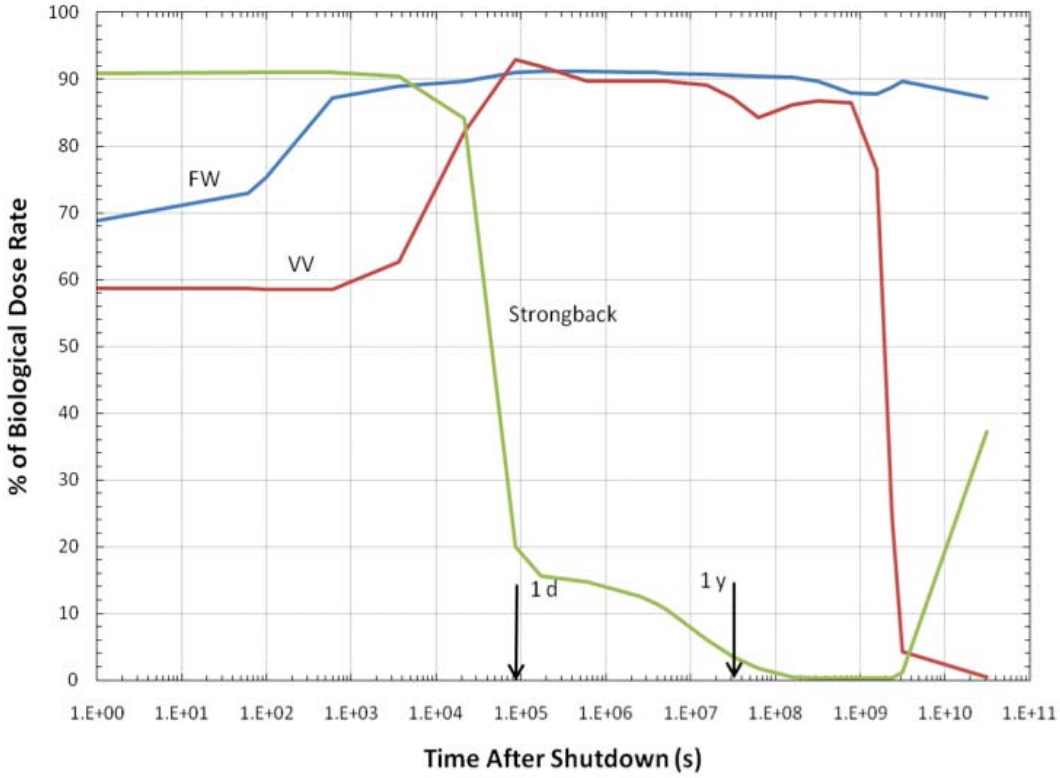

Figure 13. Contributions of FW, VV, and strongback to the biological dose rates calculated behind these components.

about one day to one year, the biological dose rate calculated behind the strongback of the magnet is largely from the cryostat and bioshield (80-95%). After 100 years, the contribution to the biodose rate behind the magnet from the strongback starts to increase, reaching ~37%. This contribution is largely from Mo-93, Nb-94, and Ni-59. Approximately 46% of this biodose rate is from Nb-94 of the WP and the remaining is from Mo-93, Nb-94, and Ni-59 of the cryostat. Another feature of Fig. 13 is that the contribution to the biological dose rate behind the VV from the VV itself diminishes after 50 years. The main contributor to the dose at longer times is Nb-94 of the WP.

4. Conclusions

The accurate multi-step method of calculating the biological dose during maintenance using the adjoint gamma transport was compared to the simple, approximate method of calculating the contact dose of the nearest component. The discrepancies between results were apparent. For the highly activated component, such as the FW, the contact dose method underestimates the biological dose by a factor of 7-8, even after factoring in the gammas from nearby components. For the least activated component, such as the magnet and bioshield, the contact dose overestimates the biological dose by up to 10 fold. If the biological dose rate is largely from components other than the nearest component, large errors in the contact dose results occur. It seems that the averaging of the activity and hence, the gamma source intensity over a component, especially the fairly thick ones, incurs the largest errors for the contact dose method. Based on these results, we plan to continue using the more accurate multi-step method for any fusion design to determine the biological dose rate at the point of interest.

Acknowledgments

The authors would like to thank Profs. M. Sawan and P. Wilson of UW-Madison for their contributions and help on several issues that arose during the course of the analysis. The work was performed under the auspices of the US Department of Energy under contract #DE-FG02-98ER54462.

Appendix

The two major computer programs used to generate our biodose results were DANTSYS and ALARA. DANTSYS is a deterministic legacy code that has been succeeded by PARTISAN. This code is used to determine the neutron flux during operation and the adjoint gamma flux in the ARIES-CS radial build. ALARA is then used to determine the activation, contact dose, and biological dose.

The following procedure is used to run the adjoint case with the previously mentioned codes.

1. Run DANTSYS in forward mode to calculate the neutron flux during operation. DANTSYS generates an rtflux file that contains the neutron flux in every interval of the ARIES-CS radial build. All in-vessel components should contain their coolants and liquid breeders. The input file for DANTSYS needs to have the correct neutron source normalization in order to obtain the accurate flux during operation. ALARA uses the rtflux file for its calculations.
2. Run DANTSYS in adjoint mode with the dose detector location specified. All coolant/breeders that are not present during maintenance should be replaced by void. The desired group flux-to-dose conversion factors are specified in the input file. In this run, DANTSYS generates an atflux file with the adjoint gamma flux specified in each interval of the ARIES-CS radial build.
3. Convert the atflux file into an ASCII file using dant2alara, a utility code written for this purpose. Save this new file as either 'adjflux…1977' or 'adjflux…1991' depending on which set of conversion factors are used. The '…' refers to the component closest to the detector. ALARA uses this text file to calculate the biological dose from each gamma source in each interval of the ARIES-CS radial build.
4. In the ALARA input file 'ARIES_alara_3.9FPYbio', the name of the adjoint flux file needs to be specified as well as the volume of the detector.
5. Run ALARA with the updated input file and no coolants/breeders in the in-vessel components. This calculation usually takes 5-10 minutes. Save the output file to an appropriate name.
6. Use the summary utility to reduce the size of the output file. Save the new file as '…-sum'.
7. If it is desired to run another case with different group flux-to-dose conversion factors, only the DANTSYS input file needs to change. Once the input file is changed, repeat steps 2-6. If it is desired to run another case with a different detector, both the DANTSYS input file and the ALARA input file need to be changed. In the DANTSYS input file, specify the new detector location. Once the input file is changed, repeat steps 2-6 being careful to properly change the detector volume specified in the ALARA input file to the new detector volume.

References

1. The ARIES project: http://aries.ucsd.edu/ARIES/.
2. F. Najmabadi, A.R. Raffray, S. Abdel-Khalik, L. Bromberg. L. Crosatti, L. El-Guebaly et al., "The ARIES-CS Compact Stellarator Fusion Power Plant," Fusion Science and Technology 54, No. 3 (2008) 655-672.
3. L. El-Guebaly, P. Wilson, D. Henderson, M. Sawan, G. Sviatoslavsky, T. Tautges et al., "Designing ARIES-CS Compact Radial Build and Nuclear System: Neutronics, Shielding, and Activation," Fusion Science and Technology 54, No. 3 (2008) 747-770.
4. T.Y. Sung, W.F. Vogelsang "DKR Radioactivity Calculation Code for Fusion Reactors," University of Wisconsin Fusion Technology Institute Report UWFDM-170 (1976). Available at: http://fti.neep.wisc.edu/pdf/fdm170.pdf.
5. W.F. Vogelsang, "Radioactivity and Associated Problems in Thermonuclear Reactors," University of Wisconsin Fusion Technology Institute Report UWFDM-178 (1976). Available at: http://fti.neep.wisc.edu/pdf/fdm178.pdf.
6. E.T. Cheng, C.W. Maynard, W.F. Vogelsang and A.C. Klein, "Nucleonic Design for a Compact Tokamak Fusion Reactor Blanket and Shield," Nuclear Technology 45 (1979) 77.
7. D.L. Henderson, R.R. Peterson, G.A. Moses, "Radioactivity in the Light Ion Fusion Target Development Facility," Fusion Technology 8 (1985) 1396.
8. D.L. Henderson, G.A. Moses, R.R. Peterson, "One-Dimensional Activation and Radiological Dose Calculations for the Light Ion Fusion Target Development Facility," University of Wisconsin Fusion Technology Institute Report UWFDM-636 (1985). Available at: http://fti.neep.wisc.edu/pdf/fdm636.pdf.
9. G.A. Moses, R.R. Peterson, R.L. Engelstad, D.L. Henderson, G.L. Kulcinski, E.G. Lovell, I.N. Sviatoslavsky, J.J. Watrous, R.E. Olson, D.L. Coo, "Preconceptual Design of the Light Ion Beam Fusion Target Development Facility," University of Wisconsin Fusion Technology Institute Report UWFDM-664 (1985). Available at: http://fti.neep.wisc.edu/pdf/fdm664.pdf.
10. D.L. Henderson, "DKR-1100: A Univac 1100 Version of the DKR Radioactivity Code," University of Wisconsin Fusion Technology Institute Report UWFDM-671 (1986). Available at: http://fti.neep.wisc.edu/pdf/fdm671.pdf.
11. D.L. Henderson, "DKRDOSE and DKRCONVERT: A Dose Rate Calculation Code and an Auxiliary Data Handling Code for the DKR and DKR-1100 Radioactivity Codes," University of Wisconsin Fusion Technology Institute Report UWFDM-672 (1986). Available at: http://fti.neep.wisc.edu/pdf/fdm672.pdf.
12. Q. Wang, O. Yasar, D.L. Henderson, "DKR-ICF: A Radioactivity and Dose Rate Calculation Code Package (Volume 1)," University of Wisconsin Fusion Technology Institute Report UWFDM-714 (1986). Available at: http://fti.neep.wisc.edu/pdf/fdm714.pdf.
13. D.L. Henderson, O. Yasar, "DKR-ICF: A Radioactivity and Dose Rate Calculation Code Package - Volume 2: Sample Problems for the DKR, CONVERT and DOSE Codes,"

University of Wisconsin Fusion Technology Institute Report UWFDM-714a (1986). Available at: http://fti.neep.wisc.edu/pdf/fdm714a.pdf.

14. O. Yasar, M. Sawan, D.L. Henderson, G.A. Moses, "Radiological Dose Calculations for the Chamber and Diode Region of the Light Ion Fusion Target Development Facility," Proc. 12th Symposium on Engineering Problems of Fusion Research, Monterey, CA, IEEE Cat. No. 87CH2507-2, Vol. 2 (1987) 877.
15. D. Henderson, M. Sawan, G. Moses, "Radiological Dose Calculations for the Diode Region of the Light Ion Fusion Target Development Facility," Fusion Technology 13 (1988) 594.
16. H. Khater, M. Sawan, "Dose Rate Calculations for a Light Ion Beam Fusion Laboratory Microfusion Facility," Proc. IEEE 13th Symposium on Fusion Engineering, Knoxville, TN, IEEE Cat. No. 89CH2820-9, Vol. 2 (1989) 1412.
17. H.Y. Khater et al., "Safety Analysis for "SOMBRERO": A KrF Laser Driven IFE Reactor," Fusion Technology 21 (1992) 2023.
18. H.Y. Khater et al., "Environmental and Safety Aspects of "OSIRIS": A Heavy Ion Beam Driven IFE Reactor," Fusion Technology 21 (1992) 2138.
19. M.E. Sawan, L.A. El-Guebaly, H.Y. Khater, "Assessment of Personnel Accessibility in the Particle Beam Fusion Accelerator Facility PBFA-II," Proceedings of the 15th IEEE Symposium on Fusion Engineering, October 11-14, 1993, Hyannis, MA (1993) 942.
20. Q. Wang, D.L. Henderson, "RACC-Pulse: A Version of the RACC Radioactivity Code for Pulsed/Intermittent Activation Analysis," University of Wisconsin Fusion Technology Institute Report UWFDM-980 (1995). Available at: http://fti.neep.wisc.edu/pdf/fdm980.pdf.
21. H.Y. Khater, "Activation Analysis of the PULSAR-I Fusion Power Reactor," Proceedings of 16th IEEE/NPSS Symposium on Fusion Engineering, Champaign IL (1995) 990.
22. H.Y. Khater, "Activation Analysis of the PULSAR-II Fusion Power Reactor," Proceedings of16th IEEE/NPSS Symposium on Fusion Engineering, Champaign IL (1995) 994.
23. H.Y. Khater, M.E. Sawan, "Radiological Dose Calculations for the Particle Beam Fusion Accelerator Upgrade (PBFA-U)," Fusion Engineering and Design 28 (1995) 730.
24. H.Y. Khater, R.T. Santoro, "Radiological Dose Rate Calculations for the International Thermonuclear Experimental Reactor (ITER)," Fusion Technology 30 (1996) 1528.
25. H.Y. Khater, L.J. Wittenberg, "Environmental and Safety Assessment of the LIBRA-SP: A Light Ion Fusion Power Reactor," Fusion Technology 30 (1996) 1584.
26. P. Wilson, D. Henderson, "ALARA: Analytic and Laplacian Adaptive Radioactivity Analysis: A Complete Package for Analysis of Induced Activation - Volume I," University of Wisconsin Fusion Technology Institute, UWFDM-1070 (1998). Available at: http://fti.neep.wisc.edu/pdf/fdm1070.pdf.
27. P. Wilson, D. Henderson, "ALARA: Analytic and Laplacian Adaptive Radioactivity Analysis: A Complete Package for Analysis of Induced Activation - Volume II," University of Wisconsin Fusion Technology Institute, UWFDM-1071 (1998). Available at: http://fti.neep.wisc.edu/pdf/fdm1071.pdf.

28. V. Khripunov, R.T. Santoro, H.Y. Khater, “Profit from Borating Concrete in the ITER Biological Shield,” Proceedings of the 17th IEEE/NPPS Symposium on Fusion Engineering, October 6-9, 1997, San Diego, CA (1998) 991.

29. H. Khater, M. Sawan, “Preliminary Radiological Assessment of the Fusion Ignition Research Experiment (FIRE),” Proc. IEEE 18th Symposium on Fusion Engineering, Albuquerque, NM, IEEE Cat. No. 99CH37050 (1999) 475.

30. H.Y. Khater, M.E. Sawan, R.R. Peterson, “Assessment of Personnel Accessibility in the X-1 Facility,” Fusion Technology 39 (2001) 1003.

31. M.E. Sawan, H.Y. Khater, “Nuclear Analysis of the FIRE Ignition Device,” Fusion Technology 39 (2001) 393.

32. M.E. Sawan, H.Y. Khater, S.J. Zinkle, “Nuclear Features of the Fusion Ignition Research Experiment (FIRE),” Fusion Engineering and Design 63-64, (2002) 547-557.

33. H.Y. Khater et al., "ARIES-ST Safety Design and Analysis," Fusion Engineering and Design 65, No. 2 (2003) 285.

34. L. Ku, J.G. Kolibal, “Radioactivation Characteristics of the Tokamak Fusion Test Reactor,” Nuclear Technology/Fusion 4 (1983) 586-598.

35. S.L. Liew, L.P. Ku, “Two-Dimensional Calculations of the Prompt and Delayed Radiation Fields of a 2.1m CIT Design,” Proc. 13th Symposium on Fusion Engineering, Knoxville, TN, Vol. 1 (1989) 120-123.

36. L.P. Ku, “Monte Carlo Calculations of Delayed Gamma-Ray Dose Rate in Complex Geometry Using the Concept of Effective Delayed Gamma-Ray Production Cross Section,” Nuclear Science and Engineering 107 (1991) 114-130.

37. L.P. Ku, S.L. Liew, “Space and Time Dependent Radioactivity Distribution in TFTR Coolant,” Proc. 15th Symposium on Fusion Engineering, Hyannis Port, MA (1994) 305-308.

38. L.P. Ku, S.L. Liew, “Global Dose Rate in TFTR Due to Neutron Induced Residual Radioactivities During DT Operation,” Proc. 15th Symposium on Fusion Engineering, Hyannis Port, MA (1994) 313-316.

39. M. Youssef, A. Kumar, M. Abdou, H. Khater, M. Sawan, D. Henderson, “Assessment of Dose Rate Profiles and Accessibility Inside the Building of the Experimental Fusion Reactor, ITER, During Operation and After Shutdown,” Fusion Engineering and Design 42 (1998) 155-172.

40. J.F. Latkowski, “Neutron Activation of the NIF Final Optics Assemblies and Their Effect Upon Occupational Doses,” Fusion Technology 34 (1998) 767-771.

41. S. Brereton et al., “Decommissioning Plan for the National Ignition Facility,” Fusion Technology 34 (1998) 1041-1046.

42. A.P. Belian, J.F. Latkowski, E.C. Morse, “Experimental Studies of Concrete Activation at the National Ignition Facility Using the Rotating Target Neutron Source,” Fusion Technology 34 (1998) 1028-1032.

43. J.F. Latkowski, J.J. Sanchez, L.C. Pittenger, “Neutronics and Activation Analysis for the National Ignition Facility Cryogenic Target Positioner,” Fusion Technology 35 (1999) 255-259.

44. J.F. Latkowski, “Occupational Dose Estimates for the National Ignition Facility,” Proceedings of the First International Conference on Inertial Fusion Sciences and Applications (2000) 831-838.

45. J.F. Latkowski, J. Sanz, “Elemental Analysis of As-Built Concrete and Aluminum for the National Ignition Facility and Their Effect Upon Occupational Dose Rates,” Proceedings of the First International Conference on Inertial Fusion Sciences and Applications (2000) 858-861.

46. J.F. Latkowski, “Measurement of the NIF Gunite Shielding Composition and Implications for Neutron Activation and Worker Doses,” Fusion Technology 39 (2001) 956-959.

47. K. Seidel, Y. Chen, U. Fischer, H. Freiesleben, D. Richter, S. Unholzer, “Measurement and Analysis of Dose Rates and Gamma-Ray Fluxes in an ITER-Shutdown Dose Rate Experiment,” Fusion Engineering and Design 63-64 (2002) 211-215.

48. Y. Chen, U. Fischer, “Rigorous MCNP Based Shutdown Dose Rate Calculations: Computational Scheme, Verification Calculations and Applications to ITER,” Fusion Engineering and Design 63-64 (2002) 107-114.

49. J. Sanz, R. Falquina, A. Rodriguez et al., "Monte Carlo Uncertainty Analyses of Pulsed Activation in the National Ignition Facility Gunite Shielding," Fusion Science and Technology 43 (2003) 473-477.

50. J. Latkowski, R. Abbott, R. Laning, S. Manson, K. Morris, S. Reyes, E. Williams, “Experience with Conversion of CAD to Monte Carlo Particle Transport Models,” Fusion Science and Technology 52, No. 4 (2007) 807-811.

51. R. Pampin, A. Davis, “Novel Tools for Estimation of Activation Dose: Description, Preliminary Comparison and Nuclear Data Requirements,” United Kingdom Atomic Energy Authority Report, UKAEA-FUS-549 (2008).

52. M.Z. Youssef, R. Feder, K. Thompson, I. Davis, G. Failla, “Benchmarking the Three-Dimensional CAD-Based Discrete Ordinates Code ATTILA using Integral Dose-Rate Experiments and Comparison to MCNP Results”, Fusion Science and Technology 56, No. 2 (2009) 718-725.

53. L. Dauffy, H. Khater, S. Sitaraman, S. Brereton, "Activation Analysis of the Final Optics Assemblies at the National Ignition Facility," Fusion Science and Technology 56 (2) (2009) 736.

54. H. Khater, S. Brereton, "Radiological Assessment of Target Debris in the National Ignition Facility," Proceedings of the 23rd Symposium on Fusion Engineering, June 1-5, 2009, San Diego, CA, ISBN # 978-1-4244-2636-2 (2009).

55. R.E. Feder, M.Z. Youssef, “Nuclear Heating and Interspace Dose Rates for the Generic ITER Diagnostic Upper Port Plugs,” Proceedings of 23rd Symposium on Fusion Engineering, SOFE-09, May 31-June 5, 2009, San Diego, CA, USA. To be published in (2010).

56. M.Z. Youssef, R. Feder, “3-D Assessment of Nuclear Heating, Dose Rate, and Structural Damage in the Generic ITER Diagnostics Upper Port Plugs and Adjacent TF Coils,” to be published in Fusion Engineering and Design (2010).
57. H. Khater et al., “Impact of Target-Material Activation on Personnel Exposure and Radioactive Contamination in the National Ignition Facility,” IEEE Transactions on Plasma Science, In Press (2010).
58. S. Sitaraman, L. Dauffy, H. Khater, S. Brereton, "Neutron Activation of NIF Final Optics Assemblies," Journal of Physics: Conference Series, In Press (2010).
59. “American National Standard for Neutron and Gamma-Ray Flux-to-Dose-Rate Factors,” American Nuclear Society, ANSI/ANS-6.1.1-1977 (1977).
60. “American National Standard for Neutron and Gamma-Ray Fluence-to-Dose Factors,” American Nuclear Society, ANSI/ANS-6.1.1-1991 (1991).
61. R.A. Forrest, FISPACT-2007 Manual, United Kingdom Atomic Energy Authority Report, UKAEA-FUS-534 (2007).
62. “American National Standard for Gamma-Ray Attenuation Coefficients and Buildup Factors for Engineering Materials,” American Nuclear Society, ANSI/ANS-6.4.3-1991 (1991).
63. R.G. Jaeger, E.P. Blizard, A.B. Chilton et al., “Engineering Compendium on Radiation Shielding,” Publisher: Springer-Verlag, New York (1970).
64. R. Alcouffe et al., “DANTSYS: A Diffusion Accelerated Neutral Particle Transport Code System,” Los Alamos National Laboratory Report, LA-12969-M (1995).
65. D.L. Aldama, A. Trkov, “FENDL-2.1 Update of an Evaluated Nuclear Data Library for Fusion Applications,” International Atomic Agency Report INDC(NDC)-467 (2004).
66. A. Pashchenko, H. Wienke, J. Kopecky, J. Sublet, R. Forrest, “FENDL/A-2.0, Nuclear Activation Cross Section Data Library for Fusion Applications,” International Atomic Agency Report IAEA-NDS-173 (1998).